Percolation disorder in viscous and nonviscous flow through porous media

J. S. Andrade, Jr.,[1,2] D. A. Street,[3] T. Shinohara,[3] Y. Shibusa,[3] and Y. Arai[3]
[1]*Cybernet Systems Co., Ltd., Nissay Otowa Building, 2-15-6 Otsuka, Bunkyo-ku, Tokyo 112, Japan*
[2]*Departamento de Física, Universidade Federal do Ceará, 60451-970 Fortaleza, Ceará, Brazil*
[3]*Department of Production Technology, Showa Denko K. K., 13-9 Shiba Daimon, 1-Chome, Minato-ku, Tokyo 105, Japan*
(Received 30 November 1994)

The complete set of Navier-Stokes equations has been numerically solved for two-dimensional random pore networks subjected to site percolation disorder. Both viscous and nonviscous flow regimes have been investigated to emphasize the effect of structure and phenomenology on deviation from the classical Darcy law of permeability. It is shown that near the percolation threshold, different scaling laws apply for distinct flow conditions. At this transition region, discrepancies in the critical exponents reflect the influence of the convective momentum transfer mechanism on the overall behavior of the disordered physical system.

PACS number(s): 47.55.Mh

I. INTRODUCTION

Porous media are very common in nature and represent important materials with several applications in engineering, physics, chemistry, and biology. Technological processes involving porous materials include petroleum exploration and production, catalysis, spread of hazardous wastes, chromatography, etc. For single-phase fluid flow, the permeability of a porous medium k is a fundamental index being generally expressed in terms of Darcy's law

$$V=-\frac{k}{\mu}\frac{\Delta P}{L}\ , \tag{1}$$

where V is the average fluid velocity (filter velocity), μ is the viscosity of the fluid, L is the length of the sample in the macroscopic flow direction, and ΔP is the pressure drop applied across the system. Equation (1) is a phenomenological model which does not account explicitly for the structural details of the porous medium at the microscopic and mesoscopic levels. As a consequence, the permeability coefficient does not exclusively depend on the porosity but also on the connectivity of the pore space and the tortuous aspect of the flow field. Furthermore, it is well known that Darcy's law with a constant permeability coefficient for a particular porous medium only applies at viscous flow conditions. This corresponds to low values of the Reynolds number, as defined by

$$\mathrm{Re}=\frac{\rho d_p V}{\mu(1-\varepsilon)}\ , \tag{2}$$

where d_p is the average particle size, ρ is the fluid density, and ε is the porosity of the medium. Several attempts have been made to predict fluid permeability by means of empirical relationships [1], semianalytical techniques [2–5], and well-known cross-property relations [6–10], especially between the permeability and electrical conductivity (formation factor) of the porous medium. Direct computational simulation based on previous knowledge of the pore space morphology can be regarded as a very promising methodology [11–13]. For instance, recent study by Martys, Torquato, and Bentz [13] has been devoted to the calculation of viscous flow permeability for different classes of random porous media which might closely resemble real materials. They were able to demonstrate that a simple scaling ansatz can be used to obtain universal permeability curves for random packings of nonoverlapping or overlapping spheres.

At high Reynolds numbers, however, convective transport becomes relevant and turbulence can play a decisive role in affecting the overall momentum transfer in the interstitial void volume. In this situation, the permeability concept can still be adopted to quantify the *resistance to flow* of a given porous medium for different physical conditions. Generally speaking, deviations from Darcy's law become gradually more significant at increasing Reynolds values where the above mentioned effects are noticeable. Results from numerical solutions of the Navier-Stokes equations for various simple channel shapes also indicate that the extent of these deviations might be strongly dependent on the pore geometry [1]. A controversial point refers to the physical interpretation of the breakdown of Darcy's law. It has been argued that the effect of inertial forces on the flow (convection) is the single mechanism responsible for the transition between the viscous regime of validity of Darcy's law and the remaining variable permeability zone at high Reynolds numbers [1]. Accordingly, the incidence of turbulence in a porous medium will only occur at much higher Reynolds values than those in the range of incipient nonlinearity.

In the present study, the main purpose is to evaluate the effect of convection in the overall flow behavior of percolationlike porous structures. The picture of site percolation disorder in a two-dimensional square lattice is adopted here as a conceptual framework for the pore space morphology. Although artificial, this is a convenient geometrical model because it presents very interesting and well established features which can be closely related with properties of real pore structures. We show that outside the range of validity of Darcy's law and at porosities approaching the percolation threshold

topology ($\varepsilon \rightarrow \varepsilon_c$), different scaling relations shall apply for different values of the Reynolds number. The dependence of the critical permeability exponent on the fluid flow conditions will then be substantiated in terms of a detailed analysis and visualization of several computational experiments.

II. MODEL FORMULATION

The detailed topology of a real porous network is extremely difficult to model. As a consequence of the resulting description for the pore space connectivity, the calculation of transport properties in such complex structures usually requires an enormous computational effort. In contrast to previous studies, the approach here is to emphasize the *phenomenological* features of the model and capture its general behavior. This can be accomplished by adopting a regular square lattice as a simplified topological representation of the system. In this case, the picture of site percolation disorder represents the natural language to study the porosity influence on the fluid flow characteristics of the system [14,15]. Simulations have been performed with 50×50 networks randomly generated to produce several different prescribed porosities. Periodic boundary conditions are used to reduce the finite-size effect on the transverse direction of the lattice. Figure 1 shows a typical realization of the porous medium.

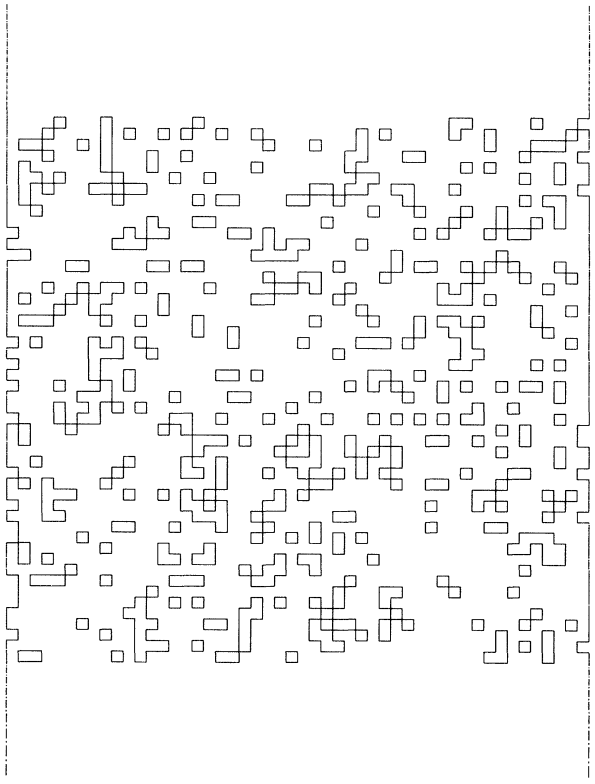

FIG. 1. A typical realization of the porous medium ($\varepsilon = 0.8$).

Apart from the pore space which is the main feature under investigation, a header and a recovery region are included to minimize end effects on the calculated flow field. The results of our simulations show that such disturbances are particularly significant in systems of low porosity. The length of these ancillary zones also seems to be an important factor influencing the stability of the numerical method. In the case where only a limited number of fluid pathways through the structure is observed, a situation which is typical of low porosity realizations, strong jets of fluid may emerge from the porous medium into the exit zone. A sufficiently large length is thus necessary to damp the jet, otherwise the gradientless boundary condition imposed at the exit will exert an adverse influence on the velocity flow field. In this study, the exit zone was set to be 2.5 times larger than the depth of the packing. This proved to be enough to ensure a negligible rate of change for the velocity vector at the outlet position.

At this stage, a brief account is given of the mathematical model utilized to describe the detailed fluid mechanics in the interstitial void space. An adequate mathematical representation should not only reveal the velocity and pressure inside the network, but also how these variables are influenced by the physical properties of the fluid and structure of the porous media. With these considerations in mind, the most suitable approach for modeling such problems is to consider the fluid as a continuum [16]. Differential balance equations for mass and momentum in an Eulerian frame of reference form the basis of the phenomenological model. In the case of a Newtonian fluid, the mathematical equations are the well-known Navier-Stokes expressions coupled with the continuity equation [17]. For isothermal and steady state flow with constant physical properties, the equations describing the local flow in the pore space of the two-dimensional percolation geometry (Fig. 1) can be written as

$$\rho\left[u\frac{\partial u}{\partial x}+v\frac{\partial u}{\partial y}\right]=-\frac{\partial p}{\partial x}+\mu\left[\frac{\partial^2 u}{\partial x^2}+\frac{\partial^2 u}{\partial y^2}\right],$$

$$\rho\left[u\frac{\partial v}{\partial x}+v\frac{\partial v}{\partial y}\right]=-\frac{\partial p}{\partial y}+\mu\left[\frac{\partial^2 v}{\partial x^2}+\frac{\partial^2 v}{\partial y^2}\right], \tag{3}$$

$$\frac{\partial u}{\partial x}+\frac{\partial v}{\partial y}=0 .$$

The independent variables x and y describe the spatial position in the pore space whereas the dependent variables u, v, and p are the components of the local velocity vector and pressure. The two necessary physical properties are the fluid density ρ and the viscosity μ.

The terms on the left hand side represent the inertial forces, while those on the right describe the shear stresses. At low Reynolds numbers, where the inertial terms are very small in comparison with the viscous forces, their contribution can be eliminated to give the well-known linear Stokes equations.

At the solid-fluid interface surrounding the solid cells, the nonslip boundary condition is used so that the local velocity of the fluid at this position is zero. As a conse-

quence of the periodic boundaries in the transverse direction, fluid is free to leave the domain through one of the vertical edges but must reenter at the same vertical position and in the same direction on the opposite side. At the inlet, a prescribed inflow velocity is used. At the exit, the rate of change of velocity in the normal direction to the boundary is assumed to be zero (gradientless boundary condition).

For the complex geometry considered here, the control volume finite-difference technique is adequate to find an approximate solution for the mathematical model. In this method, the region in Fig. 1 is divided into a number of nonoverlapping quadrilateral elements of equal size. The size of the elements is the key parameter for obtaining a sufficiently accurate numerical solution. Obviously, a numerical scheme containing many elements of small size should be able to capture more details of the flow. However, a very refined numerical grid is usually prohibitive from the computational point of view. The parameter n refers to the number of fluid cell subdivisions utilized in the finite-difference scheme for numerical discretization of Eqs. (3). In the present study, grid element lengths with a quarter of the solid cell size ($n=4$) have been adopted in all simulations. For the calculation of the overall pressure drop in the system, this finite grid proved to generate satisfactory results when compared with a numerical scheme of small resolution ($n=2$). Figure 2 shows a close-up view of part of the utilized discretization grid in a typical porous structure.

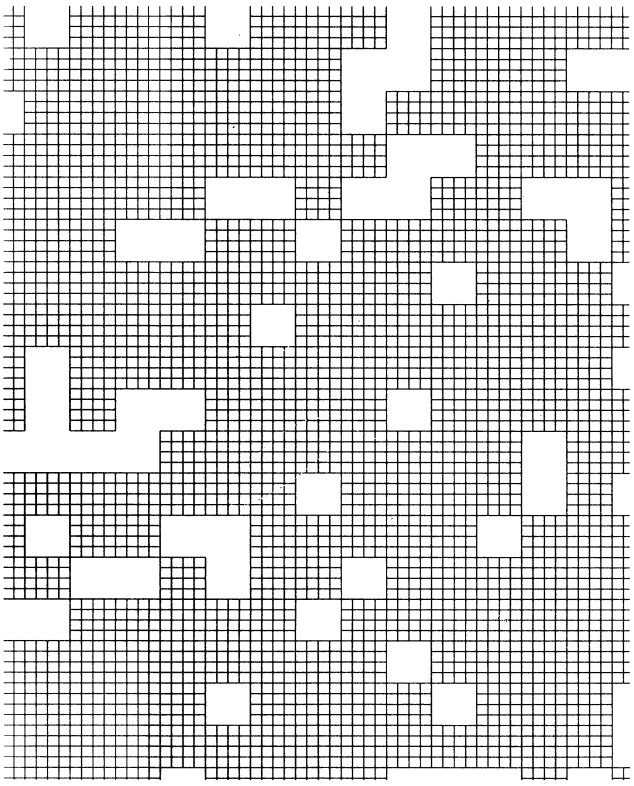

FIG. 2. Close-up view of the discretization grid utilized in a typical porous structure ($n=4$).

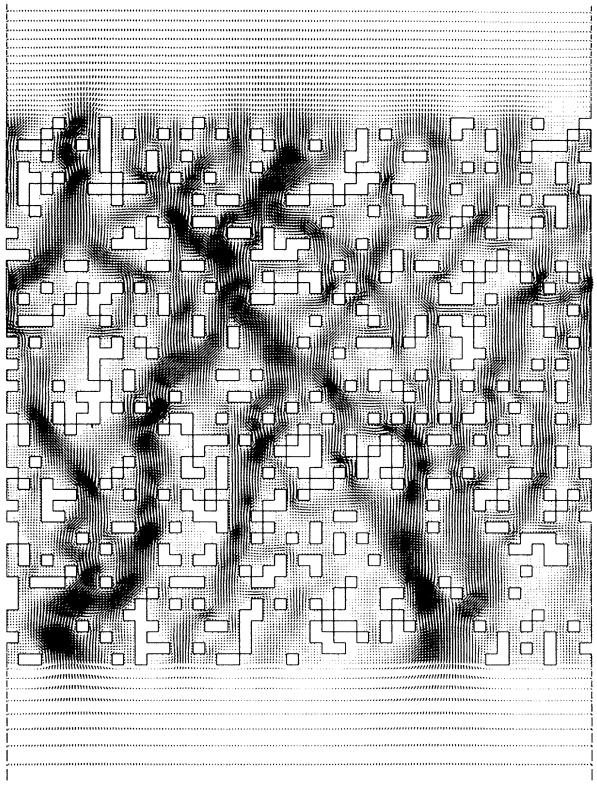

FIG. 3. Plot of the velocity flow field through a porous medium at low Reynolds number ($\varepsilon=0.8$, Re$=0.01$).

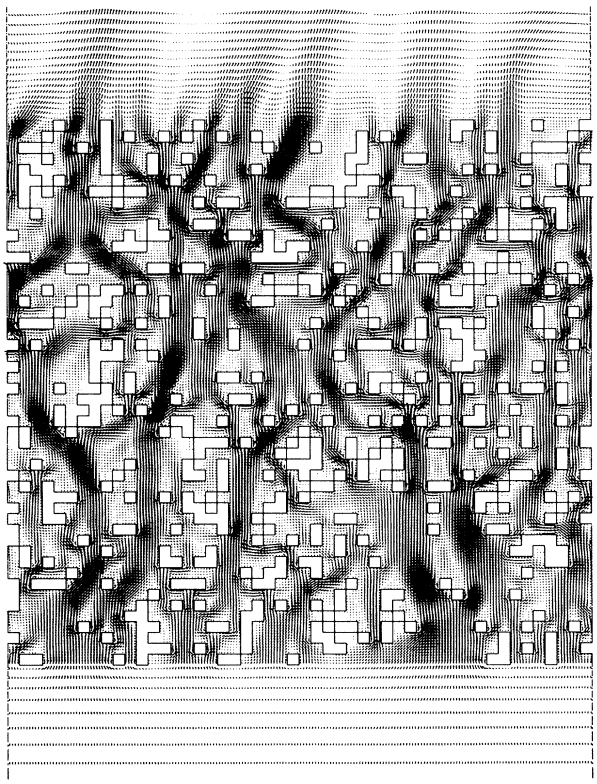

FIG. 4. Plot of the velocity flow field through a porous medium at high Reynolds number ($\varepsilon=0.8$, Re$=100$).

For each quadrilateral element in the numerical grid, the finite-difference analog of the mass and momentum balance are developed by considering the integral form of the governing equations. This gives rise to a set of coupled nonlinear algebraic equations which are pseudolinearized and solved sequentially using the SIMPLER algorithm [18]. Convergence is achieved when the sum of the momentum and mass residuals in each element falls below a specified value.

Finally, the overall pressure drop across the sample (ΔP) is calculated from the area-averaged pressures at the entrance and exit positions of the percolating porous network.

III. RESULTS AND DISCUSSION

Figure 3 shows the velocity flow field through a porous medium for a given porosity, $\varepsilon = 0.8$, and Reynolds number, $\mathrm{Re} = 0.01$. This low Reynolds value has been chosen to ensure that the inertial terms have a negligible influence on the general aspect of the flow field and global pressure drop. Even though the flow pathways form a highly connected backbone structure at this high porosity value, preferential channels can be clearly detected in such viscous flow conditions. As shown in Fig. 4, the flow patterns generated at a higher Reynolds number, e.g., $\mathrm{Re} = 100$, but with otherwise similar conditions, are significantly different from the previous case. In this situation, the degree of channeling is less intense and the velocity flow distribution is more homogeneous. Bottlenecks can still be observed, but because *the effective fluid accessibility* is enhanced by the contribution of inertial forces, *the relative maximum velocity* at these regions is lower than for purely viscous conditions. The discrepancy between flow patterns for a given porous structure at very different Reynolds numbers is an interesting feature of the simulations which could not be directly interpreted from permeability data only. From an essentially geometrical argument, well distributed flow at high Reynolds number would naturally suggest a reduced permeability coefficient, due to the less tortuous characteristic of the flow field. However, the resistance to flow is not exclusively influenced by the tortuosity of the porous medium. Although the surface area is the same in both cases, the energy dissipation in the bulk fluid phase and at the solid-fluid interface is much larger in high Reynolds number conditions than in the situation of viscous flow. Since lower permeability coefficients have been computed for high values of the Reynolds number, this effect is certainly predominant over the geometrical one. These considerations are reinforced by close-up sections of Figs. 3 and 4 which are displayed in Figs. 5 and 6, respectively. Figure 6 also confirms the occurrence of some recirculation zones where the fluid experiences rapid changes in direction. This fact indicates that convection prevails over the viscous mechanism of momentum transfer in the flow at high Reynolds values.

As shown in Fig. 7, the complicated topology of the porous structure at a low porosity value creates very tortuous pathways for fluid flow in nonviscous conditions.

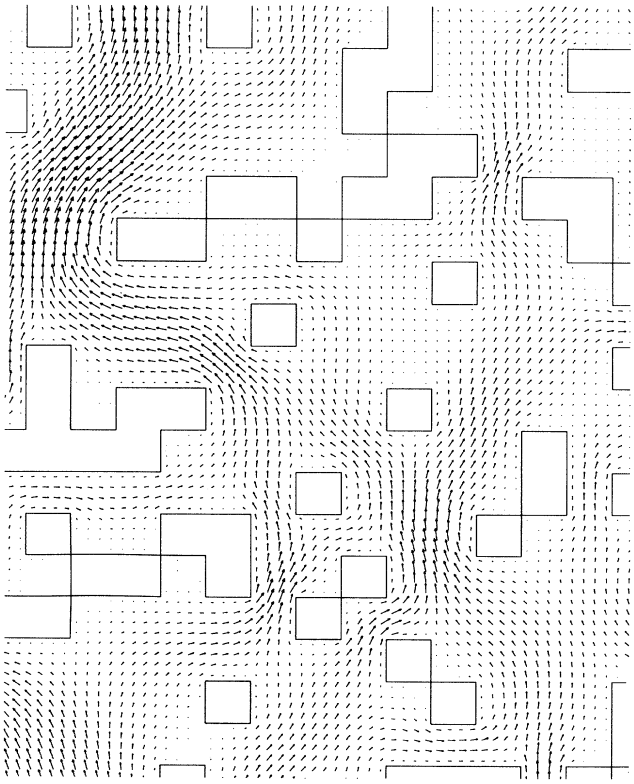

FIG. 5. Close-up section of Fig. 3.

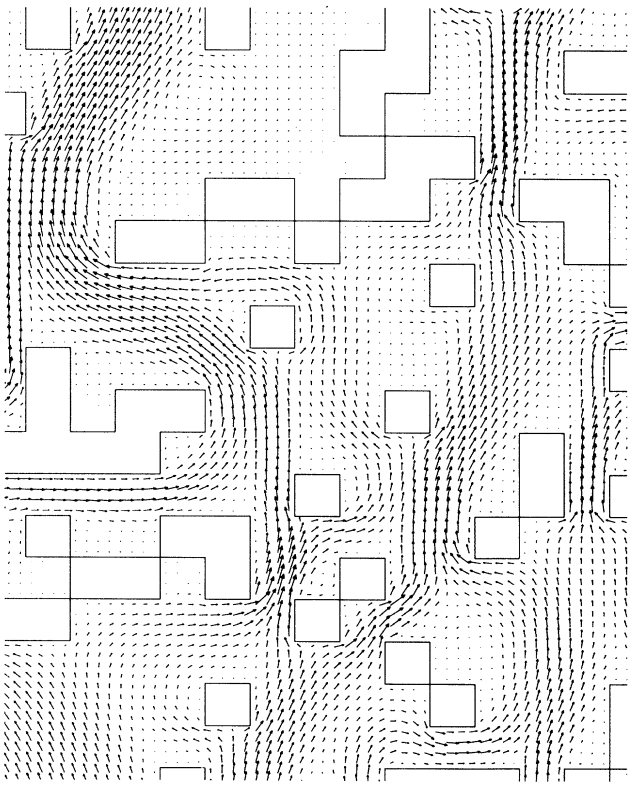

FIG. 6. Close-up section of Fig. 4.

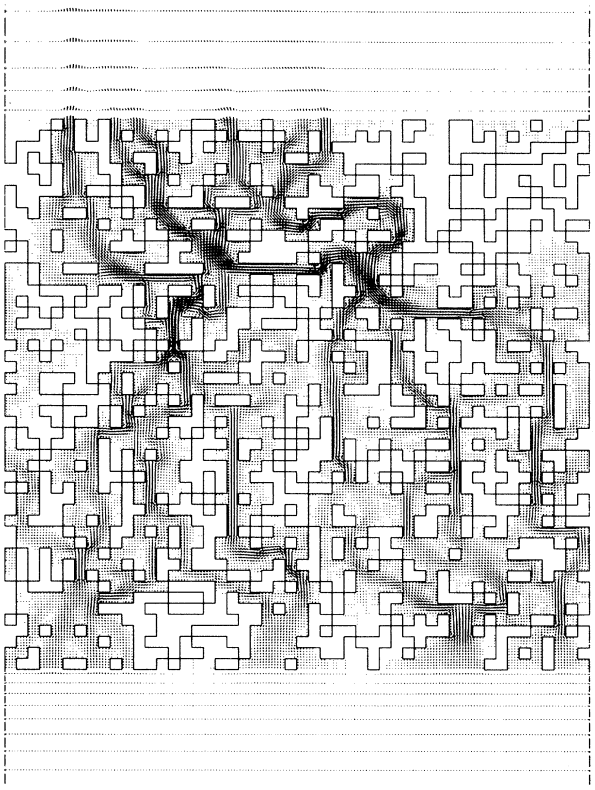

FIG. 7. Plot of the velocity flow field through a porous medium with low porosity at high Reynolds number ($\varepsilon=0.65$, $\mathrm{Re}=100$).

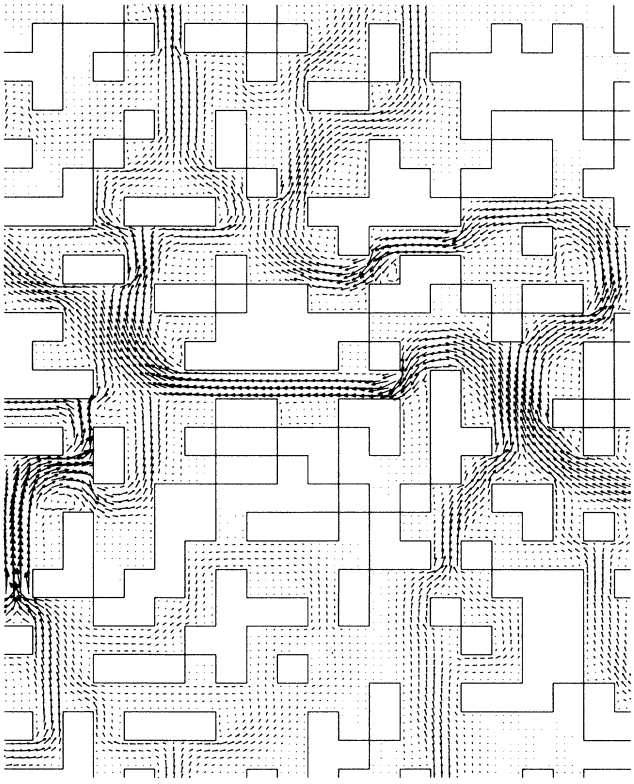

FIG. 8. Close-up section of Fig. 7.

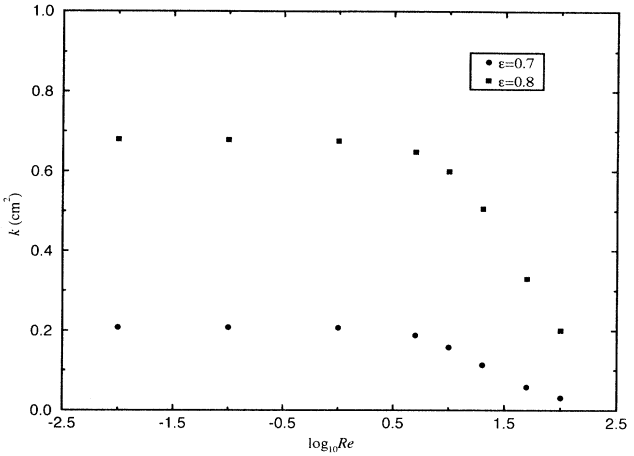

FIG. 9. Dependence of the permeability coefficient on the Reynolds number for two different values of the porosity.

In addition, several dead-end regions are present and attached to the percolation backbone. At high Reynolds numbers, the strong channeling effect due to the geometrical configuration of the system is accompanied by several recirculation zones. Furthermore, the close-up of the velocity vector field in Fig. 8 also shows that the high tortuosity of the medium can even induce the occurrence of backward fluid movement with relation to the main direction of the flow.

Figure 9 shows that for fixed porosity values above the percolation threshold, the permeability coefficient is initially constant (Darcy's law) and then gradually decreases with the increase of the Reynolds number, after a certain transition point. This behavior has already been explained in terms of the greater energy dissipation of the system in the presence of inertial forces, causing a higher resistance to flow at large Reynolds values. As a consequence, lower permeability coefficients are to be expected at high Reynolds numbers where convection is significant. Figure 10 shows the dependence of the permeability on the porosity of the medium for two different

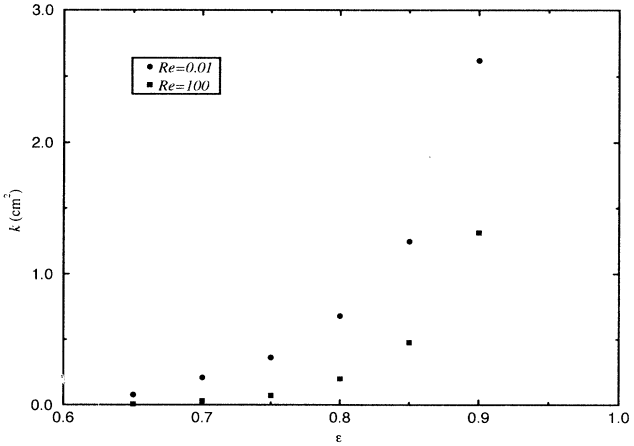

FIG. 10. Dependence of the permeability coefficient on porosity of the network for two different Reynolds values.

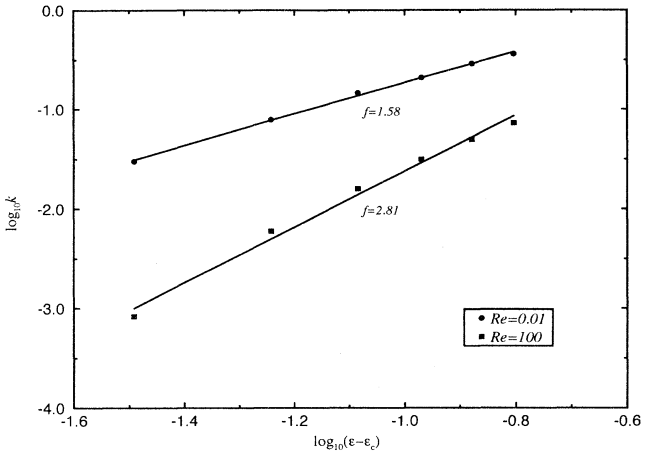

FIG. 11. Logarithmic plot of k vs $(\varepsilon-\varepsilon_c)$ for two different Reynolds values.

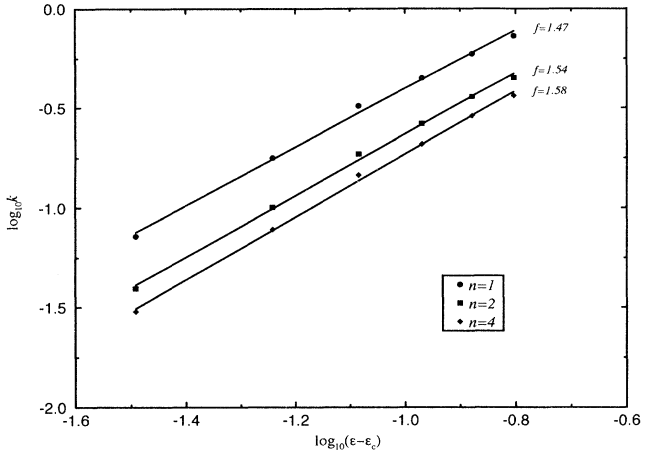

FIG. 12. Logarithmic plot of k vs $(\varepsilon-\varepsilon_c)$ for three different values of the grid discretization parameter n.

Reynolds values. A distinctive feature from these plots is that the two quantities seem to disappear with different critical exponents, though at the same threshold porosity which is a purely structural property of the system. As a consequence, when the porosity approaches the threshold value ($\varepsilon\rightarrow\varepsilon_c$, $\varepsilon_c=0.592\,746$ for the square lattice [19]) one can conjecture a power law relationship for permeability

$$k \propto (\varepsilon-\varepsilon_c)^f , \tag{4}$$

which involves the following functionality between the critical exponent and Reynolds number:

$$f=f(\mathrm{Re}) . \tag{5}$$

This nonuniversal behavior is illustrated in Fig. 11 where the result of fitting low porosity data ($0.6<\varepsilon<0.75$) with Eq. (4) is shown in a logarithmic plot. As previously mentioned, only small pore networks could be utilized in the simulations for reasons of computational feasibility. Furthermore, because of the numerical complexity of the problem, simulations for a given porosity value have been restricted to a few realizations of the disordered structure. In these circumstances, the obtained critical exponents surely do not represent accurate percolation parameters, especially due to finite-size effects. Nevertheless, it does not compromise the qualitative aspect of the results which basically aim to emphasize the fact that distinct scaling laws should represent dissimilar flow regimes near the percolation threshold. The large discrepancy between critical exponents at different Reynolds numbers clearly illustrates that the interplay between structure and phenomenology must be carefully examined in the analysis of flow permeability through porous materials. Even at viscous flow conditions, the analogy between permeability and electrical conductivity only applies if details of the pore morphology are not taken into consideration. This should be the case when, for example, an active fluid cell in our simulations is replaced by a single node of negligible volume connecting four half-channels in a typical site percolation system. It should then be possible to demonstrate that the traditional conductivity problem in percolation theory only becomes equivalent to the viscous flow permeability in pore networks when a very coarse numerical grid is adopted in the simulations. An attempt to do so is displayed in Fig. 12, where critical exponents have been calculated for permeability data at low porosity for three different levels of grid refinement. As expected, convergence on the permeability coefficient for different porosities can be achieved by increasing the parameter n, the number of grid cell subdivisions in the numerical solution. The interesting aspect of these simulations, however, is the fact that the critical exponent of the less refined grid, $f=1.47$ for $n=1$, appears to be the closest one to the reported value of the electrical conductivity exponent in two dimensions, $f=1.3$ [19]. This is compatible with our previous justification and somehow demonstrates the consistency of the methodology. The results in Fig. 12 can also be interpreted by observing that our idealized disordered system can display features of both discrete (coarse numerical grid, small n) and continuum (fine numerical grid, large n) percolation models. As a consequence, simulations with refined numerical grids would tend to produce larger critical exponents than their coarse grid counterparts, in perfect agreement with previous studies on transport phenomena in continuum percolation systems [20,21].

IV. CONCLUSIONS

The numerical simulations performed in this study have illustrated the role played by convection affecting the flow patterns in porous structures subjected to percolation disorder. It was demonstrated that the scaling law governing the percolation transition in fluid flow is intrinsically dependent on the particular aspects of the momentum transport phenomena taking place at the pore space level. In other words, above the range of validity of Darcy's law, one has to consider a nonuniversal behavior for the critical exponent relating flow permeability coefficients and porosities near the threshold zone. As a

consequence, for a given dimension, such an exponent must be a function of Reynolds number to correlate data where inertial contributions to fluid flow are relevant.

From a detailed inspection of the resulting velocity fields, it was possible to compare and analyze different features of the flow under viscous and nonviscous conditions. At high Reynolds numbers, when the convective mechanism is significant, a distinctive characteristic of the fluid flow is the occurrence of recirculation zones in dead-end spaces connected to the main stream flow paths. Backward flow could also be detected in pore networks generated at a prescribed low porosity. This was explained in terms of the highly tortuous conformation of the percolation backbone through which most of the fluid flow is observed. Further simulations with large lattices and more refined numerical grids are necessary to produce more accurate and quantitative evidence that these factors represent essential elements of the fluid mechanics in disordered porous structures. The investigation of rheological and turbulence effects on the fluid flow in percolationlike porous media are also part of our current research project.

ACKNOWLEDGMENTS

This work was entirely carried out at the Department of Production Technology of Showa Denko K. K.

[1] F. A. L. Dullien, *Porous Media—Fluid Transport and Pore Structure* (Academic, New York, 1979).
[2] J. Koplik, J. Fluid Mech. **119**, 219 (1982).
[3] D. Nicholson, J. K. Petrou, and N. K. Kanellopoulos, Chem. Eng. Sci. **43**, 1385 (1988).
[4] J. H. Petropoulos, J. K. Petrou, and N. K. Kanellopoulos, Chem. Eng. Sci. **44**, 2967 (1989).
[5] J. S. Andrade, Jr., F. Benyahia, E. A. Foumeny, C. McGreavy, and K. Rajagopal, Chem. Eng. Technol. **15**, 11 (1992).
[6] A. J. Katz and A. H. Thompson, Phys. Rev. B **34**, 8179 (1986).
[7] D. L. Johnson, L. M. Schwartz, and J. Koplik, Phys. Rev. Lett. **57**, 2564 (1986).
[8] J. R. Banavar and D. L. Johnson, Phys. Rev. B **35**, 7283 (1987).
[9] S. Torquato and B. Lu, Phys. Fluids A **2**, 487 (1990).
[10] M. Avellaneda and S. Torquato, Phys. Fluids A **3**, 2529 (1991).
[11] A. Cancelliere, C. Chang, E. Foti, D. H. Rothman, and S. Succi, Phys. Fluids A **2**, 2085 (1990).
[12] L. M. Schwartz, N. Martys, D. P. Bentz, E. J. Garboczi, and S. Torquato, Phys. Rev. E **48**, 4584 (1993).
[13] N. Martys, S. Torquato, and D. P. Bentz, Phys. Rev. E **50**, 403 (1994).
[14] M. Sahimi, G. R. Gavalas, and T. Tsotsis, Chem. Eng. Sci. **45**, 1443 (1990).
[15] J. S. Andrade, Jr. and K. Rajagopal, J. Phys. A **24**, L1379 (1991).
[16] G. K. Batchelor, *An Introduction to Fluid Dynamics* (Cambridge University Press, Cambridge, England, 1967).
[17] R. B. Bird, W. E. Stewart, and E. N. Lightfoot, *Transport Phenomena* (Wiley, New York, 1960).
[18] S. V. Patankar, *Numerical Heat Transfer and Fluid Flow* (Hemisphere, Washington, D. C., 1980).
[19] D. Stauffer and A. Aharony, *Introduction to Percolation Theory* (Taylor and Francis, London, 1992).
[20] B. I. Halperin, S. Feng, and P. N. Sen, Phys. Rev. Lett. **54**, 2391 (1985).
[21] S. Feng, B. I. Halperin, and P. N. Sen, Phys. Rev. B **35**, 197 (1987).